



Frequency Regulation Strategy in Islanded Microgrid With High Renewable Penetration Supported by Virtual Inertia

Gourav Kumar Suman¹ · Suman Yadav² · Josep M. Guerrero³

Received: 13 February 2024 / Accepted: 17 June 2024
© The Author(s), under exclusive licence to Springer Nature Singapore Pte Ltd. 2024

Abstract

The widespread adoption of power converter-based renewable energy sources (RESs) has led to a significant decline in overall system inertia within interconnected power systems. This reduction in inertia poses a significant challenge, as it increases the susceptibility of the interconnected power system to instability. To address this critical issue, this research proposes an application of virtual inertia control as a means to enhance the frequency stability of interconnected power systems characterized by a high penetration level of RESs. The proposed approach leverages a derivative control technique to enable higher-level virtual inertia emulation. By introducing a second-order characteristic into the virtual inertia control loop, the method emulates inertia, resulting in improved frequency stability and enhanced system resiliency. A dynamic model of microgrid linked is developed and the frequency stability is ensured by a Fractional Order Proportional Integral Derivative (FOPID) controller using Teaching Learning Based Optimisation (TLBO) algorithm. The problem is formulated with Integral Time Squared Error (ITSE) of frequency deviation for determining the controller. The performance of the developed controller is compared against conventional controllers in terms of the stability of the microgrid. In addition, the superiority of TLBO is analysed by comparing it with other well-established algorithms in the literature. The suitability is established under various scenarios of load and renewable uncertainties. Furthermore, the work also includes sensitivity verification of the controller by parametric variation of the range of $\pm 70\%$.

Keywords Virtual-inertia · Microgrid stability · FOPID · Robustness · Optimisation · TLBO

Gourav Kumar Suman and Sumna Yadav contributed equally to this work.

✉ Gourav Kumar Suman
gauravsuman283@gmail.com

Suman Yadav
sumanyd12345@gmail.com

Josep M. Guerrero
joz@energy.aau.dk

¹ Department of Electronics and Communication Engineering, Madanapalle Institute of Technology & Science, Madanapalle 517325, Andhra Pradesh, India

² Department of Electrical and Electronics Engineering, Madanapalle Institute of Technology & Science, Madanapalle 517325, Andhra Pradesh, India

³ Center for Research on Microgrids (CROM), Department of Electronic Engineering, Technical University of Catalonia, Barcelona 08019, Spain

Introduction

The increased depletion of fossil fuels and their adverse effects on the environment has caused a surge of interest in power engineers towards renewable energy resources. A dramatic increase has been observed in the number of distributed generation systems mainly due to technological advancements as well as price drops. Besides, the increased incentives by the government in certain developing countries like India have led to an increased attraction towards renewable energy-based generation systems. Concerning the above and the increased energy demand, the shift towards renewables is one of the most feasible solutions. Although beneficial, the presence of renewable energy resources in the power system causes numerous issues such as low reserve capacity, lesser inertia, higher fault currents and weaker fault ride-through capability. The two most commonly used renewable energy resources namely solar and wind energy are highly unpre-

dictable in terms of availability. Intermittency is an inherent property of renewable energy resources, thus an increased penetration of these resources in the system poses a severe challenge to the frequency stability of the system [1].

Right through the beginning of renewable energy-based systems, researchers have been in a constant attempt to develop dynamic models suitable for these systems. In one such attempt, a dynamic load frequency control (LFC) model of a diesel engine and fuel cell-based microgrid unit was proposed in [2]. The authors emphasised that a certain combination of renewable energy resources could serve as benefactors in maintaining the frequency stability of a microgrid-based system. The authors analysed the performance of the designed model by applying step variation of both the load and the renewable energy sources. The renewable energy-based generation scheme has also seen the inclusion of rapid-acting ultracapacitors as providers of energy bursts in microgrids. Authors in [3], developed an isolated microgrid system making use of ultracapacitors. The main objective of implementing an ultracapacitor was to improve the inertia of the system to stabilise the oscillations in the frequency dynamics of the system. It is worth noting that the developed microgrid consisted of both controllable and uncontrollable energy sources. As stated above, the increased penetration of renewable energy resources in a microgrid-based system weakens the overall inertia. To overcome the same, the work in [4] utilised tuning of the inertia constant of the system in the LFC dynamics of the system. The developed microgrid consisted of diesel generation as the main source of energy supported by battery energy storage systems (BESS) and ultracapacitors. The performance was analysed both for the variation in the internal system parameters and for the variation in the operating conditions. For a similar nature of stability problem, the work in [5] developed an optimal sizing scheme for BESS for a microgrid with high renewable penetration. The variables chosen for optimisation were the power and energy ratings of the BESS. A case study was done for an islanded system at 'Flinders Island' in Australia utilising the results obtained in the above optimisation. The authors emphasised optimal sizing of the battery storage system for supporting the deviations in the frequency dynamics. The work presented in [6] considered improving the frequency dynamics of a microgrid system with a high share of renewable energy resources. The authors employed a scheme for tapping the virtual inertia potential of renewable energy resources by developing a derivative control mechanism. The obtained results were validated against numerous scenarios of variation such as abrupt and variable changes in load and also for variations in renewable energy penetration. The developed model was observed to be beneficial. However, it was also noted that the photovoltaic-based virtual inertia mechanism took longer to settle the deviation in frequency compared to conventional

models of energy generation schemes. The authors placed the development of a suitable mechanism to reduce the settling time for damping the oscillations as a possible scope of work. In addition, the authors also emphasised reducing the demand for energy storage devices and PV systems for supplying impulsive energy during smaller periods. Fini et al analysed the loading aspect of a weak microgrid system in the frequency dynamics of the system [7]. The work coordinated the generation units and the connected loads to the system in such a manner that the control reserve of frequency was managed optimally. Two multiobjective optimisation problems were considered for attaining the solution for the above problem. The developed method was deemed to be feasible for the control of frequency with the variation in the inertia of the system. It is also to note that the changes in the inertia of the system presented only a feeble impact on the controller. An elevated share of Renewable Energy Resources in the power systems complicates the balancing process of the grid and hampers the operation of the market. However, certain dedicated devices may be added to the renewable energy integrated systems to support in terms of variation of power, and balancing of grids among others [8]. To begin with, the generation based on renewable energy resources is connected to the microgrids mainly implementing power electronics interfaces. These interfaces in turn are limited in terms of the delivery of power and thus could not generate inertia property, thereby reducing the inertia of the entire system. During an event of a disturbance, the inertial property plays a significant role in damping down the oscillations in the frequency deviation of the system [9]. It thus can be inferred that the presence of power electronics converters based on renewable energy generation schemes would affect the frequency stability of the system. Excessive deviation of frequency beyond the tolerable bounds may lead to an undesirable shedding of loads or a chain of events including faults, failure of equipment or protection action etc usually referred to as cascading outages in the power system. Besides, an excessive deviation in frequency may also lead to blackouts. The intermittency of renewable energy may cause continuous variation in frequency leading to a significant rise in the rate of change of frequency. This in turn may lead to the phenomenon of pole-slipping in generation units giving rise to the tripping of protection systems [10]. The technical issues faced while integrating a higher share of renewable energy resources can also be handled with numerous newly developed technologies for instance advanced control techniques and optimisation schemes.

Related Works

The threats to stability may be overcome by the development of certain auxiliary control schemes such as the inclusion of virtual synchronous control in the renewable energy-based

system. These control schemes emulate the behaviour of a basic inertial system such as synchronous generators without the need for actual rotating masses. There have been numerous instances in the literature implementing the concept of virtual inertia emulation for stabilisation of the dynamic performance of power systems. In one of the earliest attempts, the authors in [11] proposed a general scheme to emulate virtual inertia in a two-area interconnected system. The authors implemented a derivative controller to manage the stored energy of converter devices in the interconnected Automatic Generation Control (AGC) power system. The obtained results provided appreciable results in terms of reduction in peak deviation in the frequency and tie-line power, thereby improving stability. In a similar attempt in [12], the authors implemented the virtual synchronous power in HVDC links to emulate inertia in a multi-area power system. The authors reported sufficient improvement in the stability of the system with the proposed virtual synchronous power-based HVDC links. The authors in [6] attempted the provision of virtual inertia by making a solar power generation system replicate the behaviour of a conventional synchronous generator. The scheme was emphasised to enhance the power handling capacity of the microgrid system alongside the improvement of the frequency response of the system. The developed system was analysed for numerous scenarios including variation in renewable injection to the microgrid system producing effective results. However, the shortcoming of the work included the longer time duration taken by the system to stabilise the frequency deviation in the microgrid, making it necessary to seek for alternative schemes. In a similar attempt, the authors in [13], utilised derivative technique-based virtual inertia control for energy storage units linked to the system through an inverter. The performance of the system was analysed by posing disturbances to the system and the performance was reported to be fitting. The authors in [14] suggested mitigation of the fluctuation in frequency dynamics in microgrid systems caused due to the presence of phase-locked loops in the inertial simulation. The work implemented the coefficient diagram method to develop a suitable control technique making use of the Chaotic Crow Search Algorithm. The results obtained were suitable in comparison against conventional integral controllers.

From the literature, it is evident that the virtual inertia-based control system can be established by implementing energy storage systems coupled with inverters. These energy storage devices supply the additionally required inertia power in the system. This paper proposes a scheme of implementing virtual inertia control in tandem with advanced system controllers for stabilisation of frequency deviation in a renewables-based microgrid system. The work employs the derivative action of the frequency deviation to emulate virtual inertia utilising a storage unit.

Contribution of the Work

The present work involves the following major contributions:

- Implementation of FOPID based system controllers operating in tandem with virtual inertia emulation controllers
- Analysis of dynamic effects of virtual inertia in the system behaviour in terms of frequency deviation
- Comparison of the developed system with those available in the literature in terms of stability under numerous perturbations

The implementation of the controller at the time of study may have a drawback in that it requires additional computational resources. Furthermore, the developed controller must be comparable to existing controllers in terms of dependability and effectiveness of results. The work focuses on the benefits of FOPID controllers in terms of performance improvements.

System Modelling

In the most general sense, frequency stability is depicted as the balance between generation and demand. If there is a significant difference in the generation and consumption of power, there would be a deviation in the system frequency. The inequality in the power balance would cause continual deviation of the frequency. To regulate the frequency of the system within the desired tolerance bounds the difference between the generated power and the load demand must be as minimal as possible. The power flow expression of such a system can be given in terms of the load demand (P_L) and total generated power (P_G) of N units as Eq. 1,

$$P_L = \sum_{i=1}^N P_{G_i} \quad (1)$$

Implementing the swing equation describing the dynamics of power imbalance in generation-load in terms of the deviation in frequency and inertia, we obtain,

$$\Delta P_m = \Delta P_L + 2 \times H \frac{d\Delta f}{dt} + D \times \Delta f \quad (2)$$

Where ΔP_L denotes the change in demand, ΔP_m denotes the change in the mechanical power, Δf denotes the deviation in frequency, H is the inertia constant of the system and D is the damping coefficient of the load. The term $\frac{d\Delta f}{dt}$ denotes the rate of change of frequency with respect to time and is often represented by ROCOF (Rate of Change of Frequency). If the damping or the inertia of the system decreases, the deviation

in frequency and therefore, the ROCOF increases. As far as microgrids are concerned, the damping constants are smaller compared to conventional power systems. The value of inertia constant depends on the implemented synchronous units. The expression relating the inertia constant of a microgrid based system to that of the synchronous generator is given by [9] as,

$$H_s = \sum_i H_{DG_i} \times \frac{S_{DG_i}}{S_s} \tag{3}$$

Wherein H_s, H_{DG_i} respectively represent the inertia constant of the system and the DG unit in relation to their nominal power outputs (S_{DG_i} and S_s respectively). From Eq. 3, it is observed that the increased penetration of renewable energy-based Distributed Energy systems with lesser or no inertia to the microgrid system leads to a reduction in the overall inertia. The implementation of RESs, though beneficial in terms of environmental aspects deteriorates the inertial response of the overall system, thereby causing a higher deviation in frequency with change of demand. The considered system consists of a Wind Power Generation System, Bio-Diesel Generation System, Solar PV System, Battery Energy Storage System, and Superconducting Magnetic Energy Storage

System. The overall system is as shown in Fig. 1. The solid lines are implemented for exchanging the electrical energy and the system control information is depicted in dashed lines. The system base is of 15 MW. The Bio-Diesel generation system is 12 MW, The wind Energy Generation system is considered to be 7 MW, the Solar PV generation system is 6 MW and the Superconducting Magnetic Energy Storage system is considered to be 4.5 MW. The load is considered to be 15 MW. The systems implemented in the studied microgrid are detailed in the upcoming subsections.

Wind Power Generation System

Of all the available renewable energy generation schemes, the wind power generation method is considered one of the most evolved and rapidly enhancing non-conventional methods. Towards the end of 2021, the global installed wind capacity amounted to 824.87 MW compared to about 539.58 MW during the end of 2017. The total generation of power implementing wind energy has increased by about 53% in the last 5 years making it one of the most progressive technology amongst all other counterparts in the renewable paradigm. In such a system, the output depends significantly on the speed of the wind at the instant of evaluation. In general, the speed

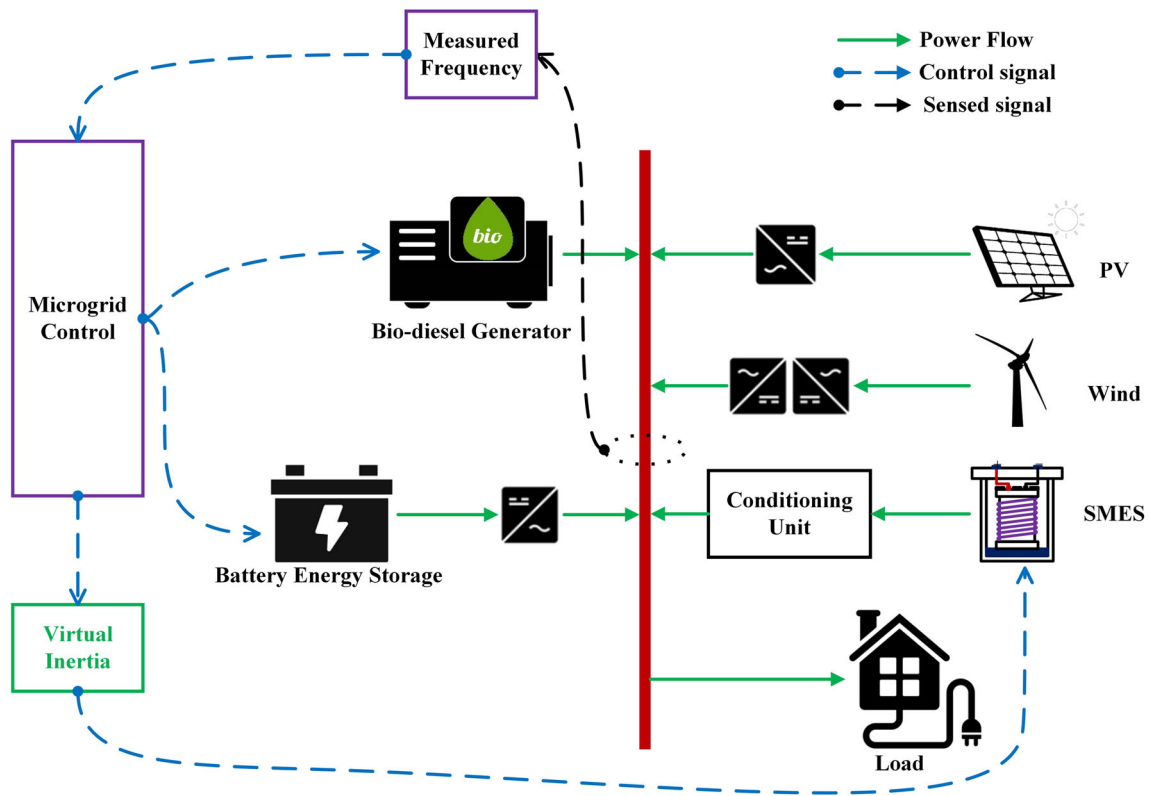


Fig. 1 Model of microgrid implementing virtual-inertia based SMES

of wind as described by authors in [15] is given as the resultant of the gust wind, ramp wind, noise wind and the base wind speed, mathematically,

$$\text{Wind Velocity} = V_b^w + V_g^w + V_r^w + V_n^w \quad (4)$$

Where, V_b^w , V_g^w , V_r^w and V_n^w respectively represent the base, gust, ramp and noise wind speed. There are several nonlinearities linked with a wind power generation unit, from adjusting the pitch angle based on wind speed to its implementation in dealing with frequency variation. The regulation of the pitch angle aids in adjusting the wind turbine's output power between its minimum and rated capacity. The first order transfer function model that ignores the non-linearities in order to study the frequency behaviour of such a system is given in Eq. 5 [16],

$$G_{wg} = \frac{K_{wg}}{s\tau_{wg} + 1} \quad (5)$$

Bio-Diesel Generation System

In its most basic form, a bio-diesel engine generation system is just a regular engine. The fuel used is what mostly distinguishes it as renewable. Biodiesel is used to power traditional diesel engines. It is derived from crops and can be used either pure or mixed. Contrary to its usual counterpart, the fuel exhibits promising performance in terms of energy output and is environmentally friendly [17]. In addition, a number of studies have promoted the use of this green energy source in place of diesel. The combustion and emission characteristics of an effective mixture of a butanol isomer and safflower extracts were emphasised by the authors in [18]. The power generated by a biodiesel system is immediately influenced by the engine's action and the input valve, in contrast to the synchronous generator of a typical diesel production unit. As a second order system, the linearized model of the internal combustion engine and valve action may be approximated as Eq. 6 [19].

$$G_{bd} = \frac{K_v K_e}{\tau_v \tau_e s^2 + (\tau_v + \tau_e) s + 1} \quad (6)$$

Solar PV System

The renewable energy source with the greatest availability is solar energy. The Solar Photo-Voltaic (PV) modules are frequently cited as one of the greatest alternative energy sources to fulfil the fast rising demand, thanks to technological advancements and the introduction of microgrids. It is important to remember that, in comparison with alternative

non-conventional energy harnessing systems, solar PV units require far less maintenance. Furthermore, these systems are environmentally friendly and noise-free. According to [20], the solar insolation and surface temperature at the place of interest determine the power produced by the solar photovoltaic module, which is expressed mathematically as Eq. 7.

$$P_{pv} = \eta \vartheta A \left[1 - \frac{\theta_a + 25}{200} \right] \quad (7)$$

η indicates the PV system's percentage conversion efficiency, ϑ represents the solar irradiance in W/m^2 , and A represents the PV system's surface area in m^2 at θ_a ambient temperatures. The linearized model of solar PV generation unit is presented as a first-order system given by Eq. 8 [21].

$$G_{pv} = \frac{K_{pv}}{s\tau_{pv} + 1} \quad (8)$$

The solar PV generating unit is not dispatchable, hence it is not involved in frequency control.

Battery Energy Storage System

Battery energy storage systems offer an efficient solution for stabilising system dynamics. In the context of renewable energy sources, which exhibit variability over time, battery units serve as suitable assets for supporting the system. The advantage of high energy density, justify their utilisation in this regard. When there is excess power generated from renewable sources, it can be used to charge the storage units. Subsequently, during periods when renewable energy sources experience a decline in power output, the stored energy can be discharged to meet the demand. In terms of mathematical modelling, the transfer function model for the battery energy storage system can be represented as 9 [22].

$$G_{bs} = \frac{K_{bs}}{s\tau_{bs} + 1} \quad (9)$$

By incorporating battery energy storage systems into the microgrid infrastructure, the stability and reliability of the system can be improved, while also enabling better integration of renewable energy sources. This approach facilitates the efficient utilisation of surplus energy and helps address the intermittency challenges associated with renewable sources. The battery energy system is considered as a dispatchable unit in this work.

Superconducting Magnetic Energy Storage system

A magnetic field created over a superconducting coil is used in magnetic energy storage systems to store energy.

Its attributes include a quick reaction time, increased power density, and extended cycle life [23]. The system includes a refrigeration mechanism to maintain the superconducting coil below the critical temperature for superconductivity [24]. The current (I) travelling through the coil generates a magnetic field proportional to its self-inductance (L). The energy that has been stored is expressed as,

$$E = \frac{1}{2} \times LI^2 \tag{10}$$

The above energy relation’s time integral represents the power that the system delivers. Aside from the cooling system and superconducting coil, the system incorporates a power conditioning system for delivering stored energy. The SMES has been created as an ideal storage system for power stability. The system is provided as a first-order transfer function as given in Eq. 11 [25],

$$G_{sm} = \frac{K_{sm}}{s\tau_{sm} + 1} \tag{11}$$

Strategy of Virtual Inertia Control Using SMES

The power generated by the virtual inertia system serves as an alternative to the actual synchronous machine [26, 27]. It is particularly useful in systems with fluctuating renewable power, as it improves frequency stability. The system compensates for the lack of physical inertia by employing a mechanism for injecting power. However, the default operational limitations of the virtual inertia device are insufficient for providing reliable frequency support. To address the non-linearities in low-inertia environments, an additional robust controller is necessary. The notion of virtual inertia control concerning the regulation of system frequency is generally based on the derivative action as presented in Fig. 2 [10].

If the derivative of the system frequency is proportionally employed to adjust the active power reference of a converter/inverter, it becomes possible to replicate inertia power within the system. This replication serves to enhance the system’s inertia response in the face of contingencies or dis-

turbances. The dynamics of the imitated active power are expressed as Eq. 12 [28],

$$\Delta P_t = J \times \frac{d(\Delta f)}{dt} \tag{12}$$

where J is the control constant expressed in terms of virtual inertia, $\frac{d(\Delta f)}{dt}$ is the deviation of variation in frequency of the system and P_t represents the imitated virtual power concerning the deviation.

The emulation of virtual inertia requires an additional energy storage device. There are numerous energy storage systems available that could be implemented for attaining the control application. Figure 3 depicts the dynamic model of a general storage based system.

However, it is worth mentioning that the response time of available energy storage systems such as batteries is slow. The work proposes an implementation of a SMES-based system which in turn bears an enhanced response time and high power compared to the earlier counterpart. The dynamic control scheme of the SMES-based system for emulation of adequate inertia in the microgrid is depicted in Fig. 4.

The derivative control technique $\frac{d\Delta f}{dt}$ is utilised to determine the Rate of Change of Frequency (ROCOF) to augment the active power set-point of the microgrid in response to contingencies. As a result, the active power generated by the SMES system is adjusted proportionally according to the system frequency variations. Consequently, the SMES would effectively emulate virtual inertia power, thereby enhancing the overall system inertia, system frequency, and performance in the context of integrating Renewable Energy Sources (RESs). The dynamic equation relating the variation in system frequency to the emulated virtual power by the SMES system is given as Eq. 13,

$$\Delta P_{smes} = \frac{J}{1 + s\tau_c} \left(K_{sm} \times \frac{d(\Delta f)}{dt} - K_{fb} \times \Delta I_d \right) (I_d + \Delta I_d) \tag{13}$$

where, P_{smes} is the emulated virtual power, τ_c is the time constant of the converter, K_{sm} is the gain of the SMES unit. I_d is the current through the inductor, ΔI_d depicts the deviation in the current due to the disturbance. k_{fb} is the negative feedback gain to ensure that the inductor current attains its

Fig. 2 Dynamic model of derivative action based inertia control scheme implementing Energy Storage System [10]

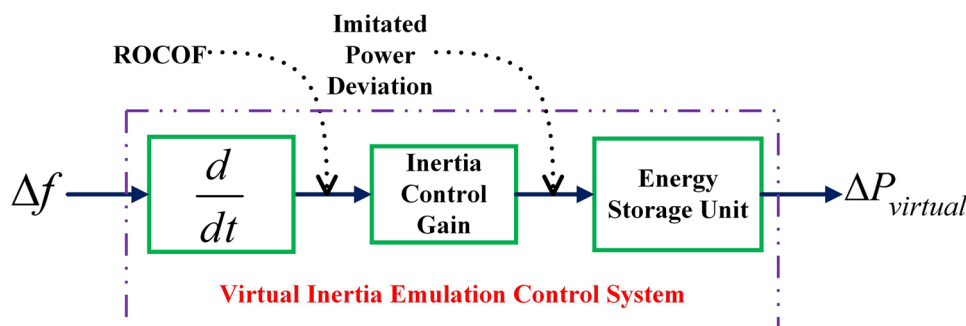
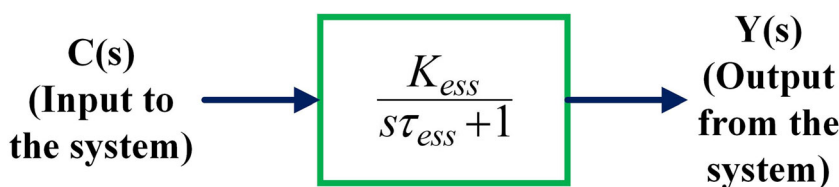


Fig. 3 Dynamic model of energy storage based inverter system [10]



nominal value after the perturbation and equip for the next disturbance. Table 1 describes the specific symbols used in modelling.

The dynamic model of the microgrid is as shown in Fig. 5.

Uncertainties

There are various sources of uncertainty in power systems. These might include changes in connected loads or changes in the amount of power provided by renewable resources. Proper modelling of the unknown parameters is important while studying the power system dynamics. It is important to remember that there is no way to precisely simulate power system uncertainties. One of the major uncertainties in the power system is the variation in connected loads, which is determined by the community’s needs and environmental conditions. The deviation model is constructed utilising the normal distribution function over the mean and standard deviation of variation. [30] defines the function as Eq. 14.

$$f(d_l) = \frac{1}{\sigma_d \sqrt{2\pi}} \times e^A \tag{14}$$

$$A = -\frac{(d_l - \bar{x})^2}{2\sigma_d^2} \tag{15}$$

Where $f(d_l)$ denotes the distribution function for load deviation, σ_d denotes the standard deviation of the load and \bar{x} represents the mean variation of the load. The work also includes analysis of the system concerning step variation,

sinusoidal variation, pulse variation and random variation to study the effectiveness of the developed mechanism.

An Introduction to the Controller Mechanism

In addition to the virtual inertia control mechanism, the present work focuses on designing a TLBO-based optimal FOPID controller for the dispatchable unit to stabilise the deviation in frequency of the developed microgrid model. As well known, fractional order calculus involves mathematical manipulation of non-integer order [31]. Of the numerous stated explanations of fractional calculus in the literature, the Caputo definition is the most widely accepted and involves the representation of the fractional order differential as Eq. 16,

$${}_a D_t^\alpha = \frac{1}{\Gamma(n - \alpha)} \int_a^t \frac{f^n(\tau)}{(t - \tau)^{\alpha - n + 1}} d\tau \tag{16}$$

It is necessary to choose an integer n such that $(n-1) < \alpha < n$. The work in [32] recommends implementing the crone from for approximating the fractional-order transfer function, which has been implemented in the current work. Since its introduction by Podlubny et al. in 1997, the parallel form of FOPID has grown in significance within the control engineering community. The controller’s time domain representation in terms of error signal ($e(t)$) is shown as Eq. 17,

$$u(t) = K_p \cdot e(t) + \int_t^\lambda K_i \cdot e(t) + K_d \cdot \frac{d^\mu}{dt^\mu} e(t) \tag{17}$$

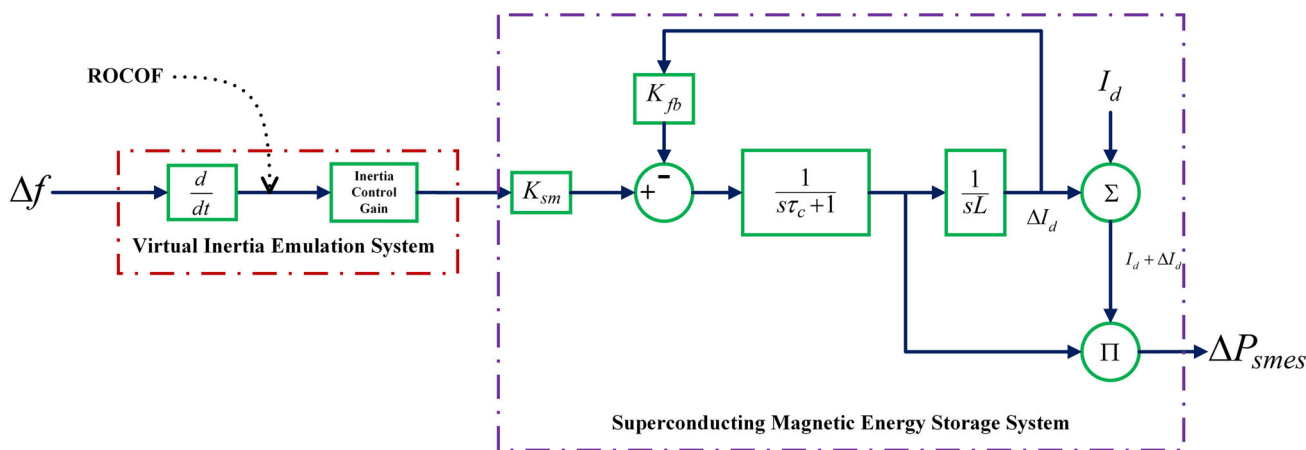


Fig. 4 Dynamic model of SMES based on virtual inertia [29]

Table 1 Terms and meanings of the symbols employed

Symbols	Nomenclature	Value
K_{wg}, τ_{wg}	gain and time constants of wind power generation unit respectively	1, 1.5 s
K_v, τ_v, K_e, τ_e	valve gain, valve actuator delay, engine gain and time constant of bio-diesel generation system	1, 0.05 s, 1, 0.5 s
K_{bs}, τ_{bs}	gain and time constants of battery energy storage unit	1, 0.1 s
K_{pv}, τ_{pv}	gain and time constants of solar PV unit	1, 1.8 s
$K_{fb}, K_{sm}, \tau_c, L$	Feedback gain, SMES control gain, converter time constant, Inductance of coil	0.2, 0.6, 10 s, 2.65 H

Where K_p, K_i and K_d respectively represent the proportional, integral and derivative control gains and λ, μ are the order operators. The Laplace transform of Eq. 17 presents the following transfer function for the FOPID controller,

$$C(s) = K_p + \frac{K_i}{s^\lambda} + K_d s^\mu \tag{18}$$

Wherein λ and μ are the order operators. A conventional PID controller can be represented by single points in the λ and μ space, however, a FOPID controller can be attained by selecting any set of orders out of the infinite possibilities. Thus, compared to a conventional PID controller with integral order, a FOPID controller bears two more degrees of freedom thereby enhancing the horizon of control design.

Formulation of the Objective Function

It is desirable to define a fitness function to be minimised to obtain optimised parameters for the above controller. The task assumed to be solved here is the stabilisation of the fre-

quency deviation. The Integral Time Squared Error of the deviation in the frequency is considered the objective function. ITSE is a combination of both the integral time absolute error and integral time squared error thereby sufficing the need in terms of the setting time as well as large oscillations in the response of the system. The fitness function is thus defined as the minimisation of Eq. 19

$$\Phi(\Gamma) = \int t[\Delta f]^2 dt \tag{19}$$

Subject to:

$$\begin{cases} \Gamma_{pmin} \leq \Gamma_p \leq \Gamma_{pmax} \\ \Gamma_{imin} \leq \Gamma_i \leq \Gamma_{imax} \\ \Gamma_{dmin} \leq \Gamma_d \leq \Gamma_{dmax} \end{cases}$$

In the above expression, Δf depicts the deviation of the frequency. The controller’s parameters are constrained within lower and higher limits. The controller gain for virtual inertia is also incorporated in the same objective function and

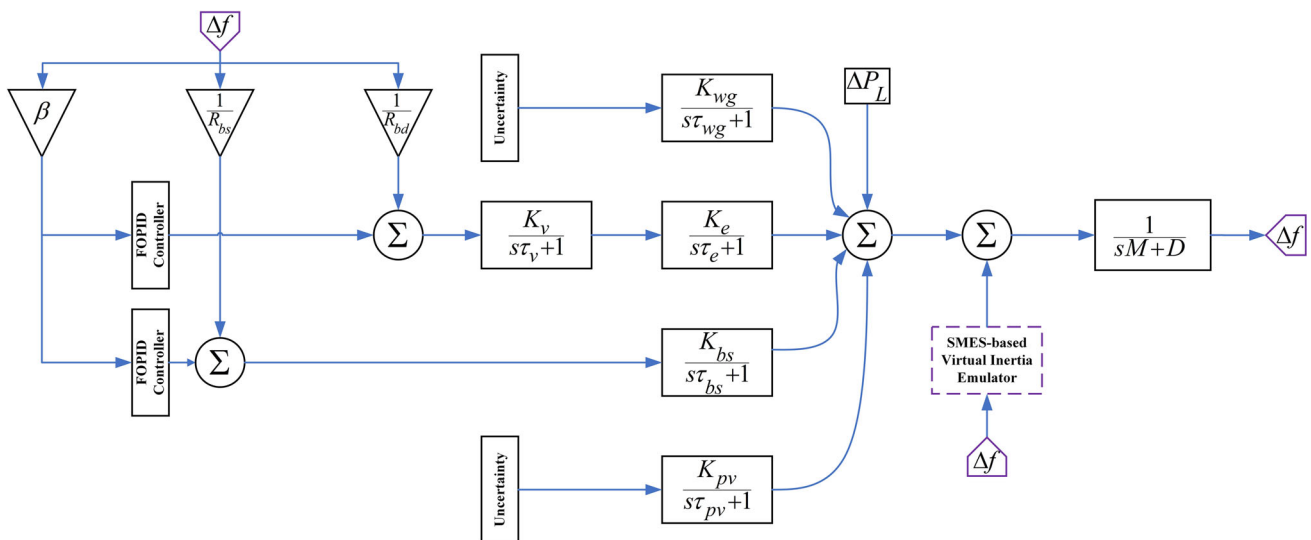


Fig. 5 Structure of the modelled microgrid

is solved for simultaneously in the process. The formulated objective function is minimised by optimisation algorithm presented in the following sections.

Optimisation Algorithms - A Summary

An optimisation algorithm finds the best collection of solutions for the fitness function stated for a given mathematical issue. The algorithm sifts through the search space to find the optimal variable combinations. Generally, an optimisation algorithm starts with an initial set of parameters and searches the user-defined search space for the best possible collection of solutions. The applicability of any solution is limited by calculating the objective function for the obtained variables in the optimisation scheme. The work implements the TLBO algorithm for the minimisation of the defined objective function. Furthermore, the performance of the implemented algorithm is compared against a few of the other well-established algorithms in the literature. The algorithms are implemented in the MATLAB environment and their codes are available in the MATLAB central library. As mentioned above, the general working of the optimisation algorithms is similar. However, the execution of the algorithms depends on the basic mathematical framework of their design. For additional insight into the mechanism of the employed algorithms, a brief has been presented in the upcoming sections.

Teaching Learning Based Optimisation

Teaching Learning Based Optimization (TLBO) is an optimization method that was introduced in 2011 and has since been widely applied to solve various engineering optimization problems, regardless of their nature [33]. It has been described in previous research [34] as a method that emulates the teaching and learning process in a classroom. In this method, the population is represented by the learners, the variables to be optimized correspond to different topics taught, and the fitness value is equivalent to the outcomes of the classroom process.

The TLBO algorithm consists of two stages: the “Teacher Stage” and the “Learner Stage.” In the Teacher Stage, the objective is to improve the mean performance of the learners based on their ability to learn from the teacher. For a given step, denoted by ‘ i ’ with ‘ d ’ variables and a population size of ‘ n ’ (where ‘ n ’ can take values from 1 to ‘ z ’), the average performance for a variable ‘ v ’ is denoted as ‘ Υ_{vi} ’. The fittest learner among the population is selected as the teacher for the subsequent stage, and their achieved results serve as inputs for the Learner Stage.

The Learner Stage involves collaboration among the learners to enhance their individual performances. When considering a pair of learners, denoted as P and Q , with different function values at the end of the previous stage, the final values of the function are obtained as Eq. 20 [34],

$$\left. \begin{aligned} & \text{If } \zeta'_{P,i} < \zeta'_{Q,i} , \\ & \zeta''_{v,P,i} = \zeta'_{v,P,i} + \vartheta (\zeta'_{P,i} - \zeta'_{Q,i}) \text{ and} \\ & \text{if } \zeta'_{P,i} > \zeta'_{Q,i} , \\ & \zeta''_{v,P,i} = \zeta'_{v,P,i} + \vartheta (\zeta'_{Q,i} - \zeta'_{P,i}) \end{aligned} \right\} \quad (20)$$

Where, $\zeta'_{P,i}$ and $\zeta'_{Q,i}$ respectively denote the values of learners P and Q at the end of first stage, $\zeta''_{P,i}$ and $\zeta''_{Q,i}$ are the modified values of P and Q at the end of the learner stage. ϑ denotes a random number between [0, 1]. The process involved in TLBO algorithm has been depicted in Fig. 6.

Particle Swarm Optimisation

The Particle Swarm Optimisation (PSO) method, created in the mid-1990s, is recognised as a well-established optimisation technique. Recent research [33, 35] shows its widespread use in engineering problem-solving. Developed by Kennedy and Eberhart, PSO imitates natural flocking behaviour. Each particle in the algorithm is controlled by parameters related to position and velocity, representing a possible solution. The algorithm explores the user-defined search space with an initial population of particles. Each particle tracks its best-found position and current location. At the end of each iteration, a velocity function updates particle positions. A random element allows particles to move to new random positions, reducing the likelihood of local minima. The objective function value for each particle is calculated at the end of each iteration, and the algorithm terminates with the predefined number of iterations.

Grey Wolf Optimiser

Mirjalili et al.’s study [36] proposed the Grey Wolf Optimizer (GWO) algorithm, inspired by the natural hunting behaviour and hierarchical structure of grey wolves. GWO begins with a pack of wolves, each representing a solution’s efficiency. Wolves are classified as alpha, beta, and delta, based on the quality of their solutions. The GWO search technique mimics how top hierarchy wolves direct hunting. An encircling equation is used to approximate the solution and explore the search area. The GWO algorithm comprises three stages:

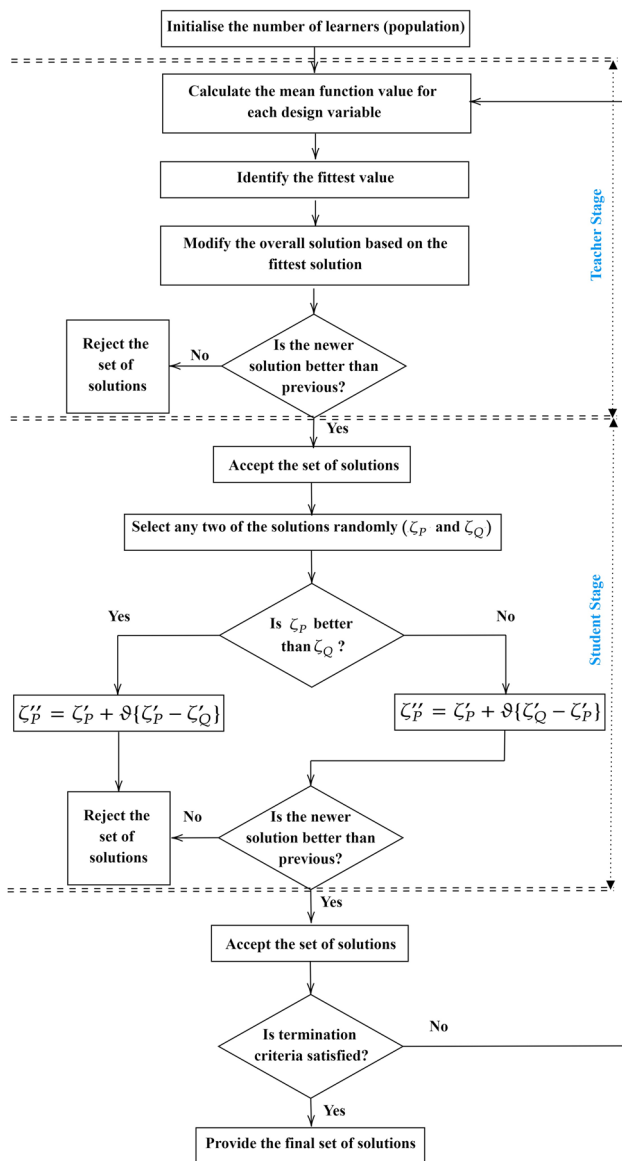


Fig. 6 Flowchart of TLBO algorithm (reproduced from authors' own work)

estimating or tracking, chasing, and attacking. The objective function determines each wolf's fitness at each iteration.

Genetic Algorithm

Genetic Algorithm mimics the process of evolution. Based on natural selection and genetics, it follows the "survival of the fittest" concept from Darwinian Theory. Developed by Prof. John Holland around 1975, it maintains a population of candidate solutions and searches the solution space by sampling. The algorithm starts with a random selection of candidates, calculates their fitness, and selects the best as parents [37]. These parents reproduce through crossover and mutation to produce the next generation, continuing until the

desired objective is met. Convergence is achieved when the objective function is attained.

Firefly Algorithm

The Firefly Algorithm, introduced by Yang in 2008, is inspired by the natural behaviour of fireflies, which use light to attract mates. In this algorithm, each firefly represents a potential solution, with its brightness indicating the quality of that solution [38]. Fireflies are attracted to each other based on brightness, adjusting their positions accordingly. The attractiveness decreases with distance, controlled by an absorption coefficient. Fireflies move towards brighter individuals to improve fitness, with a randomization parameter allowing exploration of the solution space. The algorithm iteratively updates firefly positions until a stopping criterion, such as a maximum number of iterations or a satisfactory fitness value, is met. This nature-inspired method effectively balances exploration and exploitation, making it suitable for complex optimisation problems.

Optimisation of Controller - A Comparative Study

The optimisation algorithms discussed in the previous section are utilised to obtain the parameters of the controller concerning the cost function depicted in Eq. 19. The mathematical behaviour of the mentioned algorithms is different, however, to maintain uniformity, each of them is executed for 100 iterations beginning with an initial population size of 50. The detailed settings and the elapsed time for each of the algorithms are depicted in Table 2.

The performance of the implemented optimisation algorithms compared in terms of their convergence is depicted in Fig. 7. The values of the objective function are depicted using a logarithmic scale such that the performances of the algorithms are easily traceable. From the plots, it can easily be observed that the value of the objective function obtained using TLBO surpasses other optimisation algorithms by a fair margin. It is necessary to determine the repeatability of the optimisation algorithms in the context of the problem being sought. There are numerous possible ways to obtain the significance of the performance in terms of repeatability, the most common one being the statistical measures or the convergence analysis. However, this work implements Intraclass Correlation Coefficient as an agreement between multiple executions. The Intraclass Correlation Coefficient (ICC) is a statistical measure commonly used to assess the reliability or agreement between multiple measurements or observations. In the context of optimization algorithms, ICC can be utilized to determine the repeatability or consistency of algorithmic

Table 2 Initial settings and generation wise average run-time of the optimisation algorithms

Algorithm	Parameters	Values
TLBO	Population Size	50
	Generations	100
	Computation time/gen.	15.31 s
PSO	Swarm Size	50
	Generations	100
	Inertia Weight	0.7298
	Inertia Weight damping ratio	1
	Learning coefficients (personal, global)	1.4962
GWO	Computation time/gen.	16.74 s
	Population Size	50
	Generations	100
GA	Random vector r_1 and r_2	rand(0,1)
	Computation time/gen.	19.67 s
	Population Size	50
	Generations	100
FA	Mutation Index	0.0015
	Crossover Index	0.65
	Generations	1000
	String Length	500
	Population Size	50
	Generations	100
	Randomness	0.5
Attractiveness	0.2	
Absorption	1	
Computation time/gen.	22.41 s	

performance across multiple runs. By treating each optimization run as a measurement, ICC provides a quantitative measure of agreement between the runs. Higher ICC val-

ues indicate stronger agreement and better repeatability. ICC has been widely applied in various fields, including psychology, medicine, and social sciences, to evaluate the reliability of measurements or assess the consistency of experimental results [39]. Its utilization in optimization algorithm repeatability analysis offers a robust statistical approach to ensure consistent and reliable algorithmic performance. For a set of data consisting of n data values. The ICC is given by [40] as Eq. 21,

$$ICC = \frac{1}{n\sigma^2} \sum_{i=1}^n (x_{i,1} - \bar{x})(x_{i,2} - \bar{x}) \dots \tag{21}$$

where,

$$\bar{x} = \frac{1}{2n} \sum_{i=1}^n (x_{i,1} + x_{i,2} \dots) \tag{22}$$

$$\sigma^2 = \frac{1}{2n} \left\{ \sum_{i=1}^n (x_{i,1} - \bar{x})^2 + \sum_{i=1}^n (x_{i,2} - \bar{x})^2 \dots \right\} \tag{23}$$

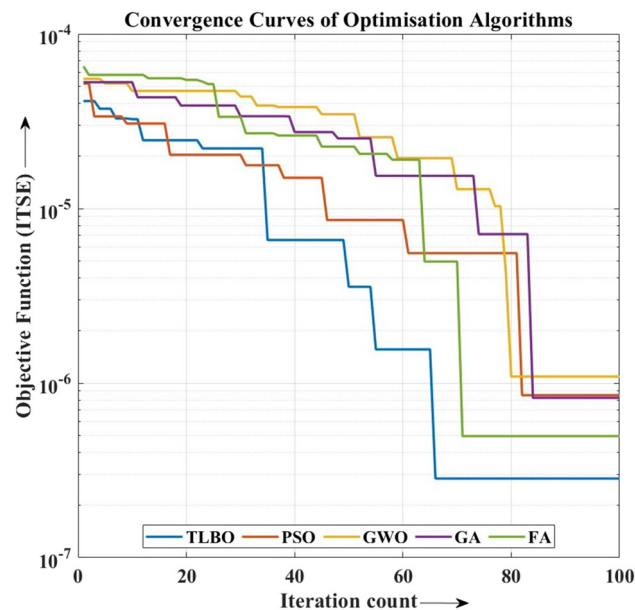


Fig. 7 Comparison of TLBO, PSO, GWO, GA and FA in terms of convergence

The optimisation algorithms are evaluated for 150 executions with 100 iterations each. The ICC computed for each of the algorithms are presented in Table 3. The significance of the algorithms are represented as good reproducibility

Table 3 Reproducibility of algorithms in terms of ICC

Algorithm	Value of ICC	Significance
TLBO	0.89	TRUE
PSO	0.92	TRUE
GWO	0.86	TRUE
GA	0.93	TRUE
FA	0.85	TRUE

for values between 0.5 and 0.75, ICC value above 0.75 are marked as excellent. It is worth mentioning that the nearness to 1 represents higher reproducibility by an algorithm. From the ICC values it can be observed that the performance of all the algorithms is commendable for the defined optimisation problem. The performance of GA surpasses all other algorithms followed by PSO and TLBO. According to the “No-Free-Lunch” Theorem (NFLT), it is theoretically impossible to have a universal optimization strategy that excels in all scenarios [41]. The only way for one strategy to outperform another is if it is specifically tailored to the problem at hand. This implies that no single algorithm can be the best performer across all domains of optimization problems. The effectiveness of an algorithm depends on how well it aligns with the characteristics of the problem domain and how efficiently it utilizes available information compared to alternative algorithms. This highlights the importance of selecting an algorithm that suits the specific application and utilizes domain-specific knowledge effectively. Considering the above evaluation of reproducibility and the NFLT, the work utilises the optimal controller obtained from TLBO algorithm for the designed hybrid microgrid system.

Comparison of the TLBO Based Controller with Conventional Controllers

The performance of the TLBO based controller is compared against those of the Tilt Integral Derivative (TID) and Proportional Integral Derivative (PID) controllers. The readers are encouraged to study the works presented in [42, 43] for details on tuning the parameters of the aforementioned conventional controllers for a chosen optimisation problem. The performance of the implemented controllers in terms of the ITSE are presented in Table 4.

Table 4 Comparison of the optimised controllers using TLBO concerning the ITSE of the frequency deviation

TLBO Controller	ITSE
FOPID	1.244×10^{-05}
PID	9.373×10^{-05}
TID	3.307×10^{-05}

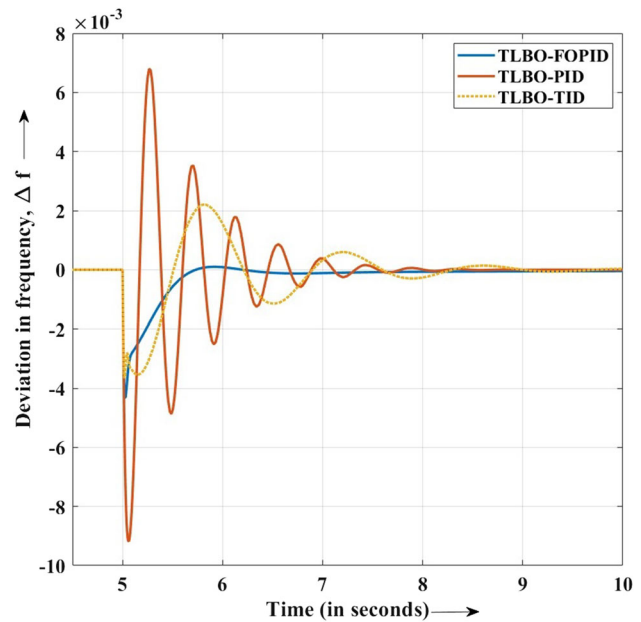


Fig. 8 Comparative frequency deviation plot of the microgrid using TLBO-FOPID for a load deviation of 10% against TLBO-PID and TLBO-TID

The behaviour of the controllers in stabilising the frequency dynamics of the system are observed for a 10% deviation in the load of the designed microgrid. The mentioned deviation is applied to the system at 5s of execution. The performance of TLBO based FOPID controller is superior compared to the other controllers. TLBO-FOPID controller gives the smallest value of the ITSE followed by TID. For a better insight on the dynamic performance of the controllers, the stability of the microgrid is observed in terms of frequency deviation for the aforementioned deviation in load. The frequency deviation is as depicted in Fig. 8.

It can be observed that the TLBO-FOPID controllers cause an overshoot of 9.96×10^{-05} pu with a settling time of 0.986s. The performance of TLBO-TID follows that of TLBO-FOPID with an overshoot of 2.2×10^{-03} pu and a settling time of 2.876s followed by TLBO-PID with an overshoot of 6.7×10^{-03} pu and a settling time of 2.946s. The lowest undershoot is observed with TLBO-TID controller followed by TLBO-FOPID controller. The time specification

Table 5 Time specifications of the frequency deviation for a 10% deviation in load under the action of TLBO-FOPID and other classical controllers in terms of their Overshoot (Os), Undershoot (Us) and settling time (ts)

TLBO Controller	Os(pu)	Us(pu)	ts(s)
FOPID	9.96×10^{-05}	-4.31×10^{-03}	0.986
PID	6.79×10^{-03}	-9.18×10^{-03}	2.946
TID	2.20×10^{-03}	-3.65×10^{-03}	2.876

Table 6 Comparison of the optimised controllers concerning the absence of Virtual Inertia Component

TLBO Controller	ITSE
FOPID	1.457×10^{-05}
PID	1.084×10^{-04}
TID	3.984×10^{-05}

of the frequency response of the microgrid model is depicted in Table 5.

The performance in terms of frequency stability as witnessed in this section establishes TLBO-FOPID as an efficient controller for the designed microgrid.

Contribution of Virtual Inertia Component

It is worth mentioning that the presence of a Virtual Inertia component in the microgrid steers the dynamics of the system to improve stability. The same has been observed by implementing the aforesaid optimisation scheme in the absence of the Virtual Inertia component. The behaviour of the system was observed for a 10% variation of the load applied at 5s of simulation time. The ITSE of the frequency deviation depicts a rise in the absence of the Virtual Inertia component. The evaluated fitness in the absence of the Virtual Inertia component is depicted in Table 6.

On comparison of the Tables 4 and 6, it is observed that the value of the fitness decreases in the presence of the virtual inertia component in the system. The ITSE of the system frequency dynamics is observed to have increased by about 17%, 16% and 20% respectively for FOPID, PID and TID controllers implementing the TLBO scheme.

Simulation and Analysis

The proposed microgrid as explained in the previous sections is developed in MATLAB®/Simulink R2023a (9.14.0.224). The implemented algorithms are developed as .m file. The simulations were performed using an Intel PC (i7-8550U CPU, 16GB RAM). The work implemented certain scenarios for analysis of the frequency control aspects of the controlled microgrid model. The scenarios are broadly classified into renewable-based scenarios, load-based scenarios and worst-case scenarios. The load based scenario is further subdivided into step variation and non-linear variation. In these scenarios the load in the microgrid is varied and the performance of the microgrid in terms of frequency deviation is observed. In the renewable based scenario the input to the renewable power generation system is perturbed and the performance of the controller is observed in terms of deviation of frequency. The last scenario namely, the worst-case scenario, the frequency deviation of the microgrid is observed by incorporating combined variation of the first two scenarios. The developed scenarios for the frequency stability studies are detailed in the following sections.

Load Based Scenarios

The step-variation in the loads of the microgrid is modelled using the normal distribution function leading to the first subset of the load based scenario. The same has been implemented mathematically as given in Eq. 14. Besides, the non-linear variation is implemented as given in [42] as Eq. 24,

$$\Delta P_L = 0.003\sin(4.36t) + 0.05\sin(5.3t) - 0.01\sin(6t) \quad (24)$$

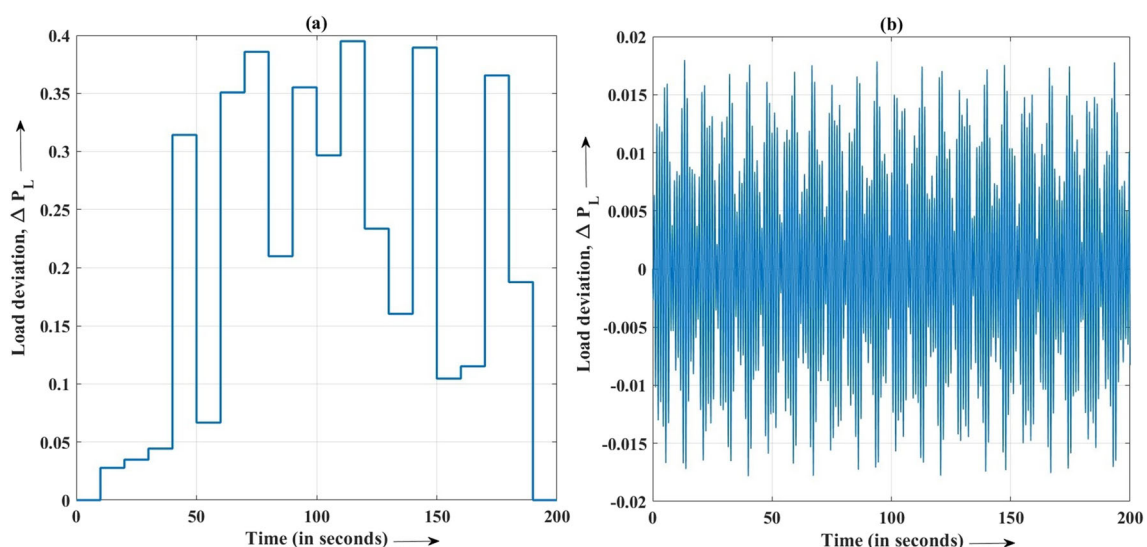


Fig. 9 (a) Scenario SI.I of step load variation in the microgrid (b) Scenario SI.II of non-linear load variation in the microgrid

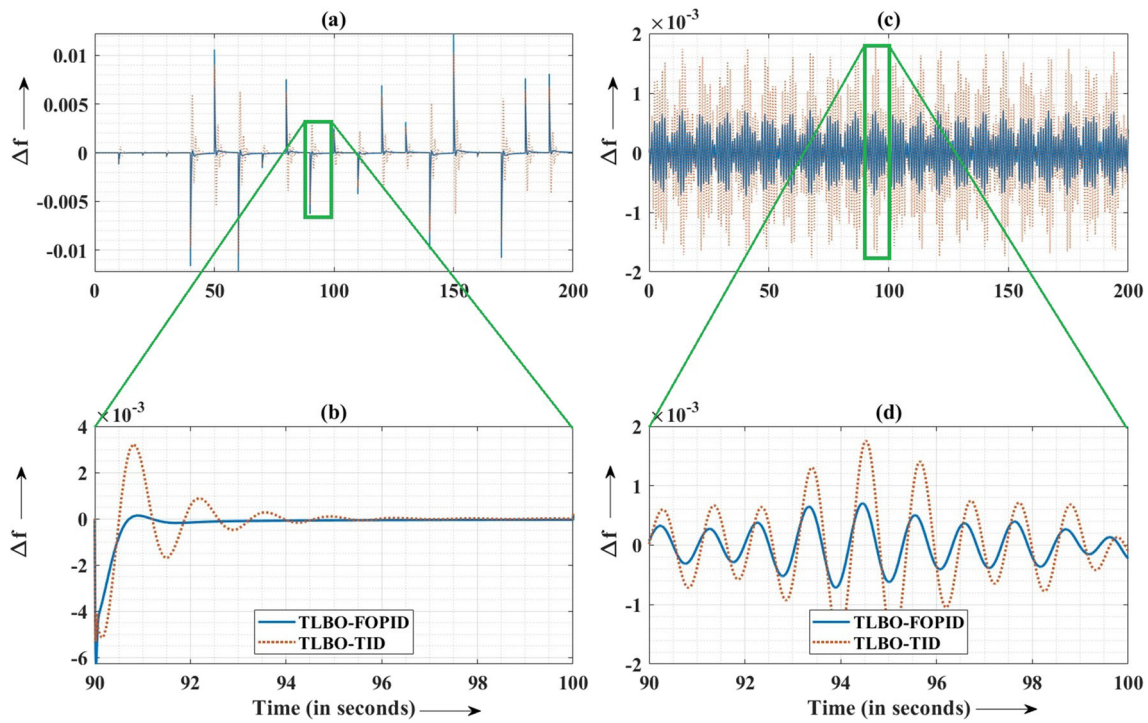


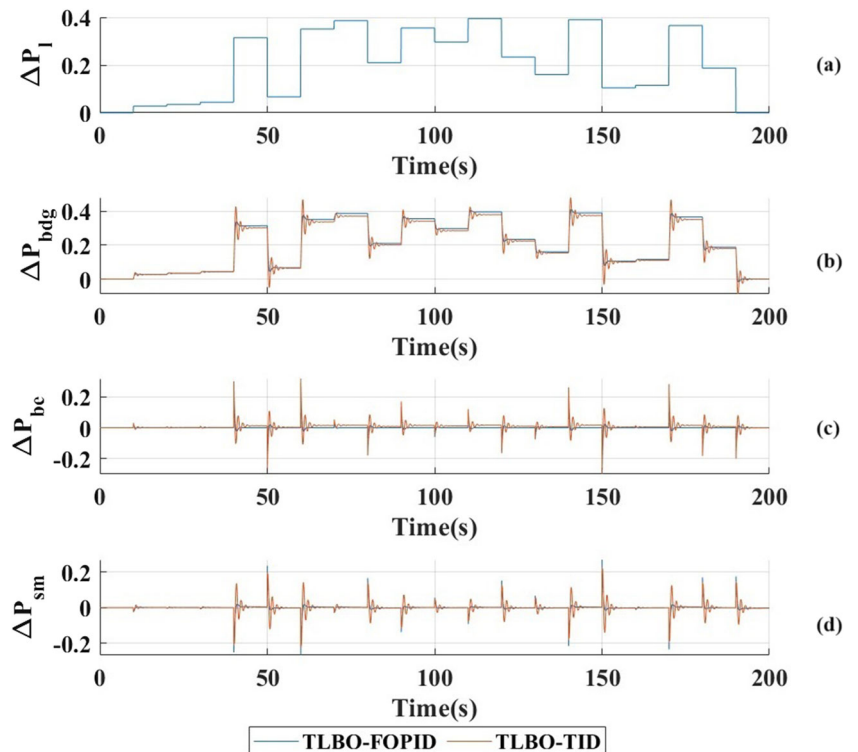
Fig. 10 (a) Frequency response of microgrid for SI.I (b) Frequency response magnified for the period 90-100s SI.I (c) Frequency response of microgrid for SI.II (d) Frequency response magnified for the period 90-100s SI.II

The cases are named as:

1. *Case SI.I* - Step variation in the load
2. *Case SI.II* - Non-linear variation in the load

The aforementioned cases are illustrated in Fig. 9 (a) and (b). It could be observed from the plots that the load variations in the microgrid are different from each other in terms of the magnitude and are distinct in their duration of occurrences.

Fig. 11 (a) Load deviation scenario SI.I (b) Variation in output of Bio-Diesel Generation (c) Variation in output of Battery Energy Storage (d) Variation in output of SMES



The frequency response for the scenarios SI.I and SI.II in the microgrid are depicted in Fig. 10 (a) - (d). The contribution of resources in sustaining the transient caused due to the variation in load for scenario SI.I is as presented in Fig. 11.

Renewable Based Scenarios

The power developed by renewable energy-based systems depends upon the input to the system, these are quite uncertain by nature. As the wind speed exhibits continuous changes concerning the weather conditions, the model developed for analysis must be designed to map the uncertainties. The above yields the significance of a probability model for wind speed variation. The work in [44] implemented the Weibull distribution function for modelling the wind speed as Eq. 25 [45],

$$f(v_w) = \begin{cases} \frac{b}{a} \times c^{b-1} \times e^{-c^b} & \text{for } v_w \geq 0 \\ 0 & \text{otherwise} \end{cases} \quad (25)$$

$$c = \frac{v_w}{a} \quad (26)$$

Where a, b respectively are the scale and the shape parameters of the distribution function and v_w represents the speed of the wind. The power generated by the system is obtained using the wind speed from Eq. 25. The relation of wind power output and the speed of the wind is given as Eq. 27 [44],

$$P_w(v) = \begin{cases} 0 & \text{for } 0 \leq v_w \leq v_{ci} \\ Pr_w \times c & \text{for } v_{ci} \leq v_w \leq v_r \\ Pr_w & \text{for } v_r \leq v_w \leq v_{co} \\ 0 & \text{for } v_w \geq v_{co} \end{cases} \quad (27)$$

$$c = \left(\frac{v_w^2 - v_{ci}^2}{v_r^2 - v_{co}^2} \right) \quad (28)$$

Where $P_w(v)$ is the generated power as a function of the wind speed, Pr_w is the power at the rated wind speed v_r , v_{ci} and v_{co} are the cut-in and cut-out speed of the wind turbine respectively. The uncertainty of solar power generation is also developed as a probabilistic model making use of the beta distribution function for the solar irradiance samples as Eq. 29,

$$f(\phi) = \frac{\phi^{\alpha-1} \times (1 - \phi)^{\beta-1}}{B(\alpha, \beta)} \quad (29)$$

$$B(\alpha, \beta) = \frac{\Gamma(\alpha) \Gamma(\beta)}{\Gamma(\alpha + \beta)} \quad (30)$$

Wherein ϕ represents the solar radiation, α and β are the shape parameters and Γ represents the gamma function. The power generated from the solar PV panels are obtained as a

relation of solar radiation (ϕ), solar radiation under standard temperature and pressure (ϕ_s) and the selected radiation point (ϕ_m) in terms of the rated power (Pr_s) as Eq. 31 [46],

$$P_s(\phi) = \begin{cases} Pr_s \times d & \text{for } 0 \leq \phi \leq \phi_m \\ Pr_s \times e & \text{for } \phi_m \leq \phi \leq \phi_{std} \\ Pr_s & \text{for } \phi \geq \phi_{std} \end{cases} \quad (31)$$

$$d = \left(\frac{\phi^2}{\phi_{std} \times \phi_m} \right) \quad (32)$$

$$e = \left(\frac{\phi}{\phi_{std}} \right) \quad (33)$$

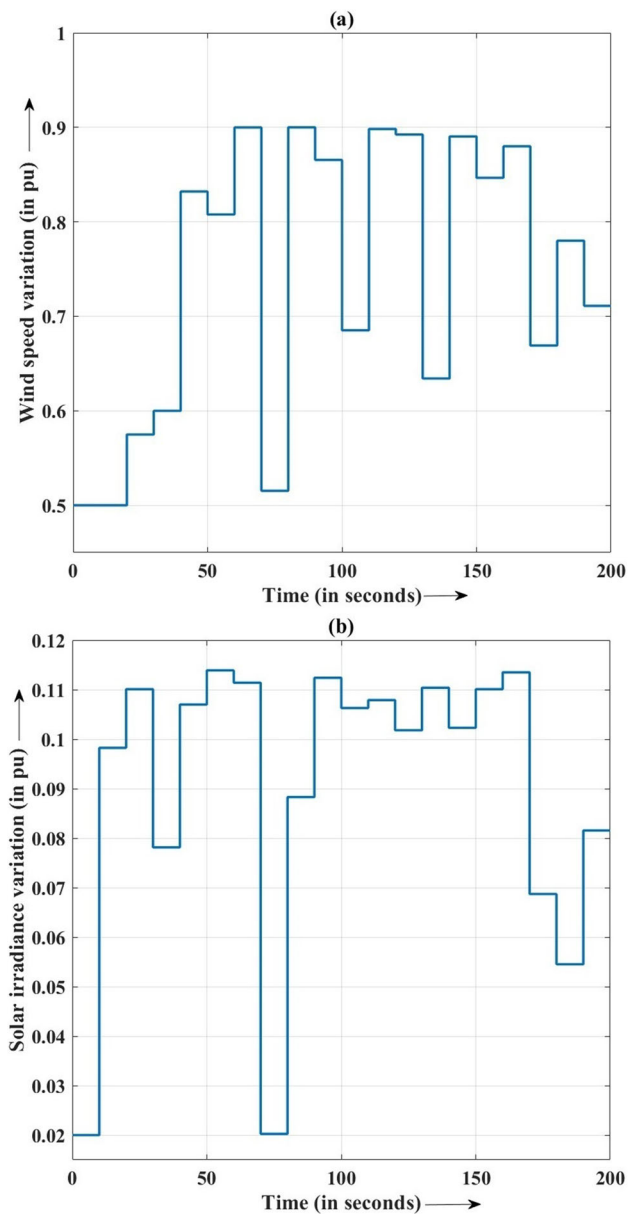


Fig. 12 (a) Scenario SI.I of variation of wind speed (b) Scenario SI.II of variation of solar irradiance

In the view of the above renewable variations, the scenario is given as

1. *Case SII.I* - Variation of the wind speed
2. *Case SII.II* - Variation of the solar irradiance

The cases mentioned above are depicted in Fig. 12 (a), (b).

The frequency response for the scenarios SII.I and SII.II in the microgrid are depicted in Fig. 13 (a) - (d).

Worst-case Scenarios

In the third set of scenarios, the combinations of variations in the first and second set of scenarios are considered. The cases formulated as as given below,

1. *Case SIII.I* - Simultaneous variation of wind and solar power generation.
2. *Case SIII.II* - Simultaneous variation of load combined with variation of wind and solar power generation.

The frequency response for the scenarios mentioned above are depicted in Fig. 14 (a) - (d).

Sensitivity Analysis

Sensitivity analysis is a crucial process that examines the impact of changes in internal parameters on the dynamic behavior of a system. In this study, the focus is on assessing

the robustness of the FOPID controller in the presence of perturbations in load and a constant deviation in renewable power generation. The optimal FOPID controller, determined through prior research, is implemented to observe the system's sensitivity to the variations of $\pm 70\%$ in the internal inertia of the microgrids. By conducting this analysis, we gain insights into the controller's ability to maintain stability and performance under different operating conditions. The frequency variation of the microgrid on the application of non-linear variation in load as expressed in Eq. 24 for the above variation is as depicted in Fig. 15. The maximum overshoot for the applied input as caused by the nominal system is observed to be 6.49×10^{-4} pu and that for the system with deviation of $+70\%$ extends to 6.6×10^{-4} pu. For the variation of -70% the overshoot observed is about 6.4×10^{-4} pu. This observation emphasises on the robustness of the obtained controller in terms of internal parametric variation. The performance of the system in terms of deviation of frequency tends to vary in the range of [1.38 - 1.69 %] for $\pm 70\%$ variation in the internal parameters of the microgrid system.

The parameters of the optimal controllers as obtained in the work are presented in Table 7.

Impact of inertia

If the effects of the mimicked virtual inertia on the system are not examined, its efforts will be insufficient. This section presents the system's time-domain performance to assess the influence of virtual inertia on its dynamic behaviour. A small-signal stability-based version of the virtual inertia is included

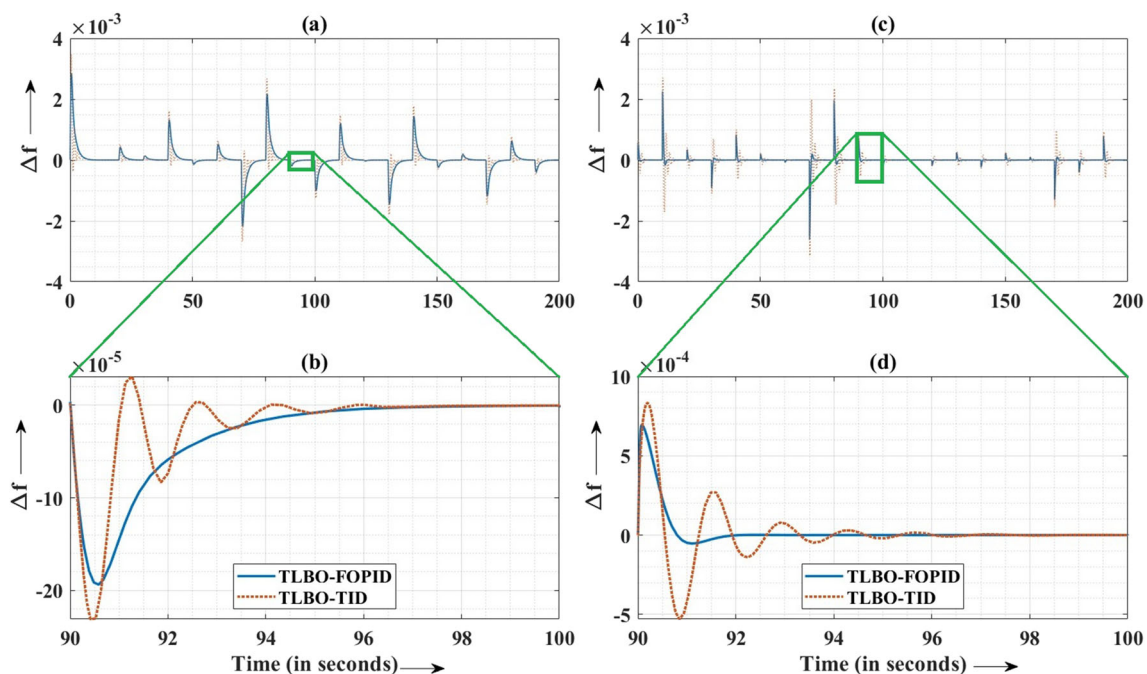


Fig. 13 (a) Frequency response of microgrid for SII.I (b) Frequency response magnified for the period 90-100s SII.I (c) Frequency response of microgrid for SII.II (d) Frequency response magnified for the period 90-100s SII.II

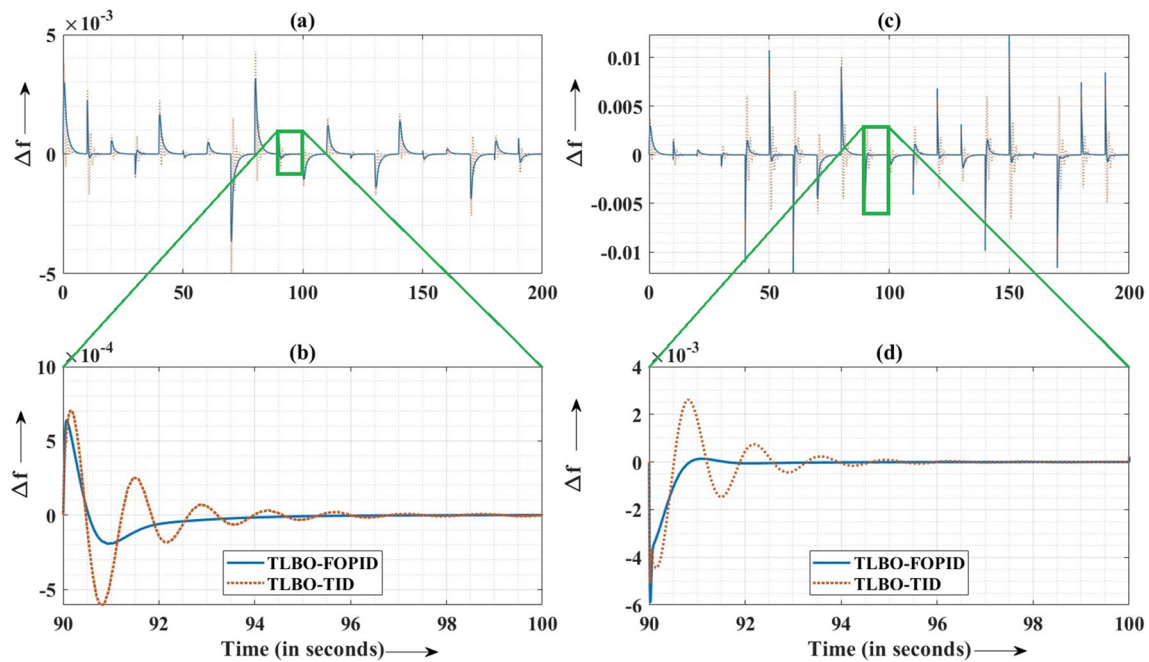


Fig. 14 (a) Frequency response of microgrid for SIII.I (b) Frequency response magnified for the period 90-100s SIII.I (c) Frequency response of microgrid for SIII.II (d) Frequency response magnified for the period 90-100s SIII.II

in the evaluation. By using a load deviation of 0.1 pu, the impact of inertia variation is examined under the nominal inertia and damping of the microgrid system. The analysis is carried out using all three controllers developed above. This ensures a comparative analysis of the controllers. The frequency deviation for the case is shown in Fig. 16.

The plot shows that increasing the value of J for the SMES unit reduces frequency transients and peak deviations. This results in enhanced frequency dynamics in a perturbed system. However, the response shows that higher inertia raises the system’s settling time. This threatens the system’s stability, hence it should be a requirement not to raise the value to

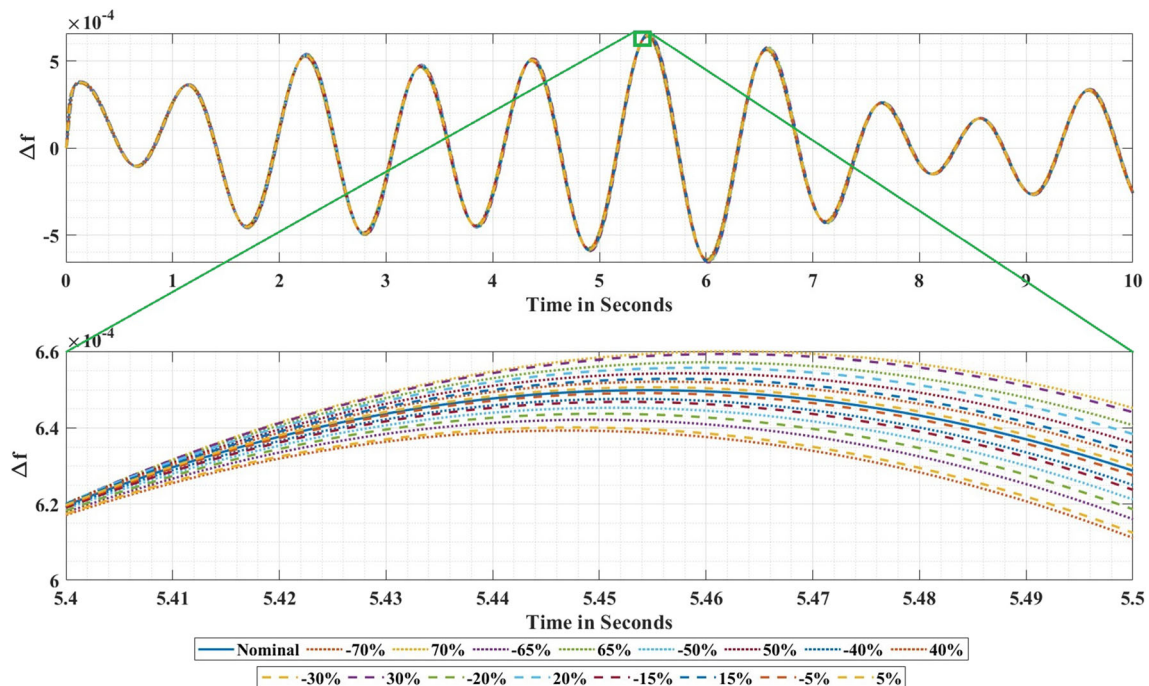


Fig. 15 Sensitivity analysis with variation in microgrid for $\pm 70\%$

Table 7 Optimal controller parameters as obtained by TLBO

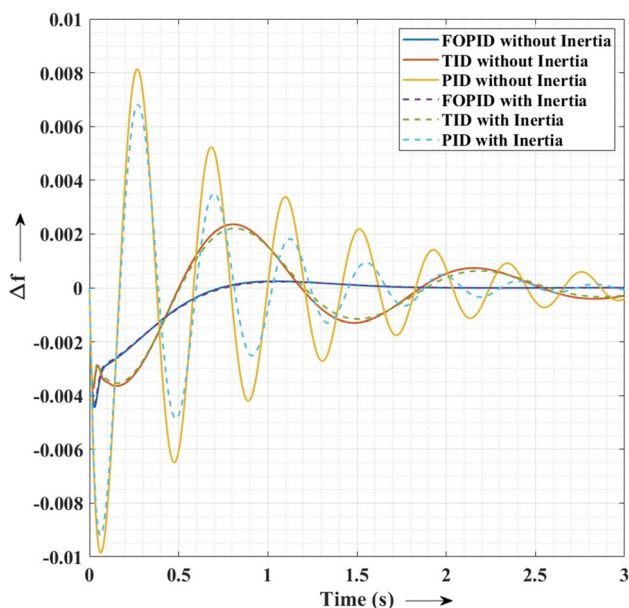
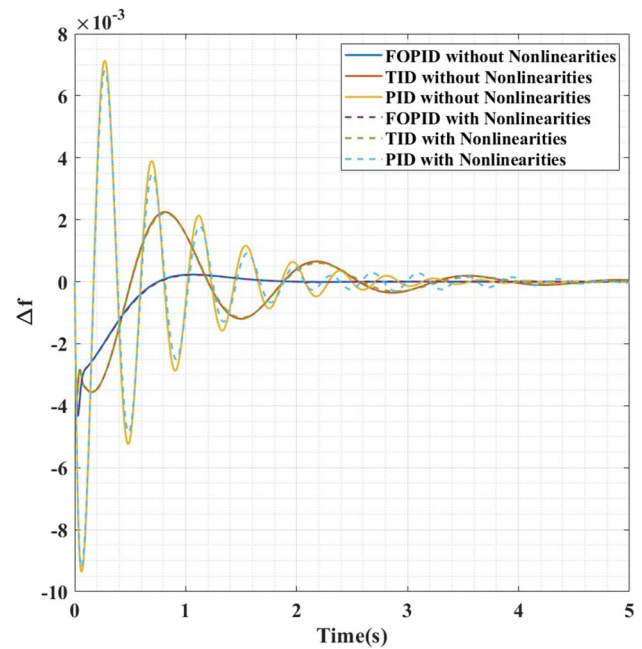
Parameters	C-I	C-II
P	-4.92	-0.68
I	-10.21	-0.62
D	-0.22	-0.61
λ	0.856	0.729
μ	0.973	0.154

a significantly larger level. It is worthwhile mentioning here, that an increase in the value of inertia of the virtual inertia emulation system deteriorates the stabilisation of the system in terms of the settling time of the dynamics.

Response with Non-linearity in the System

The dynamics of the system are verified in the presence of general nonlinearities of the electrical energy and communication systems. Nonlinearities such as the Generation rate constraint for the Bio-diesel generation system and time delay for the Virtual Inertia component of the SMES have been implemented for evaluation. For this study, the generation rate constraint is applied as 15% p.u, and the time delay of propagation for the virtual inertia-based system is specified as 1.5s. Similar to the previous case, the dynamics of the system response were analysed for 0.1pu perturbation in the load. The frequency response of the system implementing all three forms of optimal controllers is presented in Fig. 17.

The proposed TLBO-FOPID technique addresses the system's nonlinearities. The outcomes show a considerable performance improvement when compared to TLBO-TID

**Fig. 16** Effect of virtual inertia component over the frequency response of the system**Fig. 17** Effect of nonlinearities over the frequency response of the system

and TLBO-PID. This demonstrates that the technique can adapt to and limit the consequences of nonlinear dynamics. As a result, the system is more stable and robust under different operating conditions.

Conclusion

A weak microgrid system in terms of inertia and renewable energy penetration namely the Wind and Solar generation system and SMES unit is modelled. The article proposed the application of a virtual inertia-based SMES controller for stability studies of the designed microgrid system. The additional controllers implemented for the biodiesel and the battery energy storage system were attuned to utilising the TLBO algorithm. The obtained controllers were compared with conventional controllers in terms of their stability dynamics. Besides, the work also incorporated a comparative study of numerous well-established optimisation schemes alongside the TLBO algorithm. The comparison was mainly based on three scenarios, namely, the load-variation, renewable variation and the worst-case scenario, encompassing a change ΔP_L , ΔP_w and ΔP_{pv} . The significant outcomes of the work are enlisted below:

1. Model of a weak microgrid system with renewable energy sources and energy storage units is designed and analysed in terms of frequency dynamics.
2. ITSE-based objective function was formulated for the frequency dynamics for the selection of an optimal controller against frequency deviation.

3. Concerning the performance of the TLBO scheme against other optimisation methods as depicted in Fig. 7, the chosen optimisation method is inferred to be as superior. ICC analysis of the schemes infers the significance of the TLBO scheme.
4. Based on the performance of the TLBO-FOPID against other controllers developed implementing the same optimisation tool as presented in Tables 4 it is inferred that the frequency stabilisation is appreciable with the TLBO-FOPID controller.
5. The increase in the inertial parameters of the system causes a significant reduction in the value of fitness. This signifies the favourable contribution of the virtual inertia parameter to the dynamics of the system.
6. The effectiveness of the controller established in terms of the system responses as presented in Table 5 for 10% deviation in loads, establishes the superiority of the developed TLBO-FOPID over TID and PID controllers.
7. The overshoot implementing TLBO-FOPID controller is obtained as 9.96×10^{-05} pu compared to 2.2×10^{-03} pu of that of the next suitable controller (TID). A similar observation is made in terms of settling time.
8. The performance of the controller is analysed against numerous scenarios in terms of load and renewable deviation. The results depicted in Figs. 10, 13 and 14 demonstrate the effectiveness of the controller.
9. The sensitivity analysis performed for the internal parametric variation as well as the variation of the inertia of the SMES-based system as presented in Figs. 15 and 16 depicts that the aforementioned variation in the parameters does not cause significant damage to the stability of the developed system.

It is thus concluded that the presented optimisation scheme can prove to be an effective controller working in tandem with virtual inertia-based SMES for maintaining the stability of the microgrid system. The implementation of the developed mechanism may be verified for interconnection with systems with diverse energy resources, potentially with the inclusion of modern-day electric vehicles and storage technologies such as Ultracapacitors. It is worth noting that as resources rise, the computational effort required to achieve optimal configuration may inevitably increase. The horizon of the work may be developed to interconnected microgrids linked with tie-line power transmission. The future scope of work may also be extended in terms of damping rate, as it was also observed that too much of an increase in the inertia induces a sluggishness in the system, thus making it take longer to stabilise. The optimal configuration of the controller may also be tested with an advanced hybrid combination of optimisation algorithms to enhance local and global exploration.

Acknowledgements J. M. Guerrero was supported by VILLUM FONDEN under the VILLUM Investigator Grant (no. 25920): Center for Research on Microgrids (CROM); www.crom.et.aau.dk.

Author Contributions G.K.S and S.Y. wrote the main manuscript, J.M.G. Validated the work, all authors reviewed the final manuscript and the revised version of the manuscript.

Funding J. M. Guerrero was supported by VILLUM FONDEN under the VILLUM Investigator Grant (no. 25920): Center for Research on Microgrids (CROM); www.crom.et.aau.dk.

Data Availability No datasets were generated or analysed during the current study.

Declarations

Competing interests There is no competing interest of personal or financial nature to disclose.

Ethical approval Not applicable as no animal or human subjects were involved.

References

1. Aziz A, Oo AT, Stojcevski A (2018) Frequency regulation capabilities in wind power plant. *Sustain Energy Technol Assess* 26:47–76
2. Abazari A, Monsef H, Wu B (2019) Coordination strategies of distributed energy resources including fess, deg, fc and wtg in load frequency control (lfc) scheme of hybrid isolated micro-grid. *Int J Electr Power Energy Syst* 109:535–547
3. Alizadeh GA, Rahimi T, Babayi Nozadian MH, Padmanaban S, Leonowicz Z (2019) Improving microgrid frequency regulation based on the virtual inertia concept while considering communication system delay. *Energies* 12(10):2016
4. Fini MH, Golshan MEH (2018) Determining optimal virtual inertia and frequency control parameters to preserve the frequency stability in islanded microgrids with high penetration of renewables. *Electr Power Syst Res* 154:13–22
5. El-Bidairi KS, Nguyen HD, Mahmoud TS, Jayasinghe S, Guerrero JM (2020) Optimal sizing of battery energy storage systems for dynamic frequency control in an islanded microgrid: A case study of flinders island, australia. *Energy* 195:117059
6. Saxena P, Singh N, Pandey AK (2020) Enhancing the dynamic performance of microgrid using derivative controlled solar and energy storage based virtual inertia system. *J Energy Storage* 31:101613
7. Fini MH, Golshan MEH (2019) Frequency control using loads and generators capacity in power systems with a high penetration of renewables. *Electr Power Syst Res* 166:43–51
8. Dadkhah A, Bozalakov D, De Kooning JD, Vandeveld L (2021) On the optimal planning of a hydrogen refuelling station participating in the electricity and balancing markets. *Int J Hydrogen Energy* 46(2):1488–1500
9. Fathi A, Shafiee Q, Bevrani H (2018) Robust frequency control of microgrids using an extended virtual synchronous generator. *IEEE Trans Power Syst* 33(6):6289–6297
10. Rakhshani E, Rodriguez P (2016) Inertia emulation in ac/dc interconnected power systems using derivative technique considering frequency measurement effects. *IEEE Trans Power Syst* 32(5):3338–3351
11. Rakhshani E, Remon D, Mir Cantarellas A, Rodriguez P (2016) Analysis of derivative control based virtual inertia in multi-area

- high-voltage direct current interconnected power systems. *IET Gener Transm Dis* 10(6):1458–1469
12. Rakhshani E, Remon D, Cantarellas AM, Garcia JM, Rodriguez P (2016) Virtual synchronous power strategy for multiple hvdc interconnections of multi-area ac power systems. *IEEE Trans Power Syst* 32(3):1665–1677
 13. Kerdphol T, Rahman FS, Watanabe M, Mitani Y, Turschner D, Beck H-P (2019) Enhanced virtual inertia control based on derivative technique to emulate simultaneous inertia and damping properties for microgrid frequency regulation. *IEEE Access* 7:14422–14433
 14. Ali H, Magdy G, Xu D (2021) A new optimal robust controller for frequency stability of interconnected hybrid microgrids considering non-inertia sources and uncertainties. *Int J Electr Power Energy Syst* 128:106651
 15. Latif A, Das DC, Ranjan S, Barik AK (2019) Comparative performance evaluation of wca-optimised non-integer controller employed with wpg-dspg-phev based isolated two-area interconnected microgrid system. *IET Renew Power Gener* 13(5):725–736
 16. Ray PK, Mohanty A (2019) A robust firefly-swarm hybrid optimization for frequency control in wind/pv/fc based microgrid. *Appl Soft Comput* 85:105823
 17. Agarwal AK (2007) Biofuels (alcohols and biodiesel) applications as fuels for internal combustion engines. *Prog Energy Combust Sci* 33(3):233–271
 18. Celebi Y, Aydın H (2018) Investigation of the effects of butanol addition on safflower biodiesel usage as fuel in a generator diesel engine. *Fuel* 222:385–393
 19. Barik AK, Das DC (2018) Expeditious frequency control of solar photovoltaic/biogas/biodiesel generator based isolated renewable microgrid using grasshopper optimisation algorithm. *IET Renew Power Gener* 12(14):1659–1667
 20. Shankar G, Mukherjee V (2016) Load frequency control of an autonomous hybrid power system by quasi-oppositional harmony search algorithm. *Int J Electr Power Energy Syst* 78:715–734
 21. Bagheri A, Jabbari A, Mobayen S (2021) An intelligent abc-based terminal sliding mode controller for load-frequency control of islanded micro-grids. *Sustain Cities Soc* 64:102544
 22. Tan Z, Li X, He L, Li Y, Huang J (2020) Primary frequency control with bess considering adaptive soc recovery. *Int J Electr Power Energy Syst* 117:105588
 23. Zhao H, Wu Q, Hu S, Xu H, Rasmussen CN (2015) Review of energy storage system for wind power integration support. *Appl Energy* 137:545–553
 24. Akram U, Nadarajah M, Shah R, Milano F (2020) A review on rapid responsive energy storage technologies for frequency regulation in modern power systems. *Renew Sustain Energy Rev* 120:109626
 25. Dhanasekaran B, Siddhan S, Kaliannan J (2020) Ant colony optimization technique tuned controller for frequency regulation of single area nuclear power generating system. *Microprocess Microsyst* 73:102953
 26. Said SM, Aly M, Hartmann B, Mohamed EA (2021) Coordinated fuzzy logic-based virtual inertia controller and frequency relay scheme for reliable operation of low-inertia power system. *IET Renew Power Gener* 15(6):1286–1300
 27. Salama HS, Bakeer A, Magdy G, Vokony I (2021) Virtual inertia emulation through virtual synchronous generator based superconducting magnetic energy storage in modern power system. *J Energy Storage* 44:103466
 28. Khadanga RK, Das D, Kumar A, Panda S (2023) Sine augmented scaled arithmetic optimization algorithm for frequency regulation of a virtual inertia control based microgrid. *ISA Trans* 138:534–545. <https://doi.org/10.1016/j.isatra.2023.02.025>
 29. Rajamand S (2021) Load frequency control and dynamic response improvement using energy storage and modeling of uncertainty in renewable distributed generators. *J Energy Storage* 37:102467
 30. Bahmani R, Karimi H, Jadid S (2020) Stochastic electricity market model in networked microgrids considering demand response programs and renewable energy sources. *Int J Electr Power Energy Syst* 117:105606
 31. Kommula BN, Kota VR (2022) Design of mfa-pso based fractional order pid controller for effective torque controlled bldc motor. *Sustain Energy Technol Assess* 49:101644
 32. Taher SA, Fini MH, Aliabadi SF (2014) Fractional order pid controller design for lfc in electric power systems using imperialist competitive algorithm. *Ain Shams Eng J* 5(1):121–135
 33. Yadav S, Mehta RK (2021) Modelling of magnetostrictive vibration and acoustics in converter transformer. *IET Electr Power Appl* 1–16
 34. Rao RV, Savsani VJ, Vakharia D (2011) Teaching-learning-based optimization: a novel method for constrained mechanical design optimization problems. *Comput Aided Des* 43(3):303–315
 35. Aguilar MEB, Coury DV, Reginatto R, Monaro RM (2020) Multi-objective pso applied to pi control of dfig wind turbine under electrical fault conditions. *Electr Power Syst Res* 180:106081
 36. Mirjalili S, Mirjalili SM, Lewis A (2014) Grey wolf optimizer. *Adv Eng Softw* 69:46–61
 37. Gani MM, Islam MS, Ullah MA (2019) Optimal pid tuning for controlling the temperature of electric furnace by genetic algorithm. *SN Appl Sci* 1(8):880
 38. Kumar V, Kumar D (2021) A systematic review on firefly algorithm: past, present, and future. *Arch Comput Methods Eng* 28:3269–3291
 39. Marofi Z, Bandari R, Heravi-Karimooi M, Rejeh N, Montazeri A (2020) Cultural adoption, and validation of the persian version of the coronary artery disease education questionnaire (cade-q): a second-order confirmatory factor analysis. *BMC Cardiovasc Disord* 20:1–9
 40. McGraw KO, Wong SP (1996) Forming inferences about some intraclass correlation coefficients. *Psychol Methods* 1(1):30
 41. Chen H, Lin Z, Tan C (2019) Classification of different animal fibers by near infrared spectroscopy and chemometric models. *Microchem J* 144:489–494
 42. Sahu RK, Panda S, Biswal A, Sekhar GC (2016) Design and analysis of tilt integral derivative controller with filter for load frequency control of multi-area interconnected power systems. *ISA Trans* 61:251–264
 43. Padhan S, Sahu RK, Panda S (2014) Application of firefly algorithm for load frequency control of multi-area interconnected power system. *Electr Pow Compon Syst* 42(13):1419–1430
 44. Rostami Z, Ravadanegh SN, Kalantari NT, Guerrero JM, Vasquez JC (2020) Dynamic modeling of multiple microgrid clusters using regional demand response programs. *Energies* 13(16):4050
 45. Nikmehr N, Ravadanegh SN (2015) Heuristic probabilistic power flow algorithm for microgrids operation and planning. *IET Gener Transm Dis* 9(11):985–995
 46. Nikmehr N, Najafi-Ravadanegh S (2015) Optimal operation of distributed generations in micro-grids under uncertainties in load and renewable power generation using heuristic algorithm. *IET Renew Power Gener* 9(8):982–990

Publisher's Note Springer Nature remains neutral with regard to jurisdictional claims in published maps and institutional affiliations.

Springer Nature or its licensor (e.g. a society or other partner) holds exclusive rights to this article under a publishing agreement with the author(s) or other rightsholder(s); author self-archiving of the accepted manuscript version of this article is solely governed by the terms of such publishing agreement and applicable law.